

Anticorrosion Performance of Epoxy Coating Containing Phytic Acid-Doped Tetraaniline Nanoparticle

Haichao Zhao^{1,*}, Tong Liu^{1,2}, Chengcheng Jiao^{1,3}, Feng Yang³

¹ Key Laboratory of Marine Materials and Related Technologies, Zhejiang Key Laboratory of Marine Materials and Protective Technologies, Ningbo Institute of Materials Technology and Engineering, Chinese Academy of Sciences, Ningbo 315201, P. R. China

² National Materials Corrosion and Protection Data Center, University of Science and Technology Beijing, Beijing 100083, China

³ School of Materials Science and Engineering, Shenyang University of Chemical Technology, Shenyang, 110142, China

*E-mail: zhaohaichao@nimte.ac.cn (H. Zhao)

Received: 26 February 2021 / Accepted: 11 April 2021 / Published: 31 May 2021

In this work, epoxy coatings containing phytic acid-doped tetraaniline (PATA) nanoparticles for Q235 steel were prepared and their anticorrosive properties were investigated. Synthesized PATA nanoparticles were characterized by scanning electron microscope (SEM), scanning probe microscope (SPM), photoelectronic spectroscopy (XPS), and Raman test. The anti-corrosion properties of coating were studied by the open circuit potential (OCP), electrochemical impedance spectroscopy (EIS), and scanning vibrating electrode technique (SVET). The experimental results showed that the content of the PATA nanoparticle has a positive effect on the barrier ability of the epoxy matrix. The epoxy coating containing 0.25 wt% of PATA nanoparticles has superior corrosion protection property and a satisfactory self-healing effect. The self-healing effect of PATA/EP coating ascribes to the synergistic effect of the passivation of phytic acid ions and tetraaniline. As an effective anticorrosion filler, the PATA nanoparticle has the potential to apply to the field of corrosion protective coating.

Keywords: tetraaniline; phytic acid; nanoparticle; epoxy coating; corrosion resistance

1. INTRODUCTION

Corrosion is the dominating inducement of damage and scrap of various civil and industrial steel structure equipment [1]. The organic coating is regarded as one of the most efficient means for corrosion protection field via isolating metal substrate surface from corrosive species. Also, numerous studies found that organic coatings can safeguard metal substrate better by blending active pigments [2]. Conducting polymers (CPs), as a class of active pigments, are usually applied to the anticorrosion field,

such as polyaniline (PANI) [3], polythiophene [4], and polypyrrole (PPy) [5, 6]. Because of their superiorities of facile synthesis, chemical stability, and electrochemical activity, it is widely accepted that the CPs can provide a remarkable anticorrosion effect by impeding the penetration of corrosive species and inducing the formation of passive oxide films on the metal substrate surface. Nevertheless, the pure CPs often have many issues such as weak interfacial adhesion and poor solubility which dramatically affect the anticorrosion properties of organic coatings. To deal with these problems, several representative methods usually are employed in recent years of studies: 1) grafting soluble functional groups into the molecular chain [7]; 2) selection of appropriate acidic dopants [8]; 3) preparation of the well-dispersed nanoparticles [9, 10]. Another successful method was preparation of well-dispersed nanoparticle utilizing the self-assembly technique [11]. Self-assembly has been considered as a promising technology for preparing nanomaterials of π -conjugated molecules by a noncovalent interaction, e.g. ionic interaction, π - π stacking, and hydrogen bonding [12].

Tetraaniline (TANI), as a typical and promising π -conjugated molecule, has been assembled into 1-D nanofibers, 2-D nanoplates, and 3-D nanoflowers via solvent exchange method assisted by acidic dopants such as inorganic acids (HCl, HNO₃, H₂SO₄, and HClO₄) and organic acids (e.g. camphorsulphonic acid) [9, 13-17]. Therefore, it should select an appropriate acidic dopant to prepare the well-dispersed nanostructure. Phytic acid, as an eco-friendly corrosion inhibitor, has good water solubility, unique molecular structure, and metallic chelation property [18]. Phytic acid has a strong chelation effect with metal ions (Fe²⁺, Mg²⁺, Zn²⁺, Cu²⁺) and the generated chelates can deposit on the metal surface to protect the metal substrate from corrosion [8]. Figure 1 depicts the molecular structure of phytic acid and tetraaniline. Considering the corrosion inhibiting effect of phytic acid, it should be an ideal acidic dopant for TANI.

In this work, phytic acid-doped tetraaniline (PATA) nanoparticle was prepared and characterized by scanning electron microscope (SEM), scanning probe microscope (SPM), Raman spectrum, and X-ray photoelectronic spectroscopy (XPS). The effect of PATA on corrosion resistance of the resulting coating was evaluated by open circuit potential (OCP) and electrochemical impedance spectroscopic (EIS). The corrosion products were also characterized through electrochemical impedance spectroscopy (EIS), SEM and energy dispersive spectrometer (EDS). Furthermore, the self-healing capability of PATA/EP coatings' scratch was tested by scanning vibrating electrode technique (SVET) analysis.

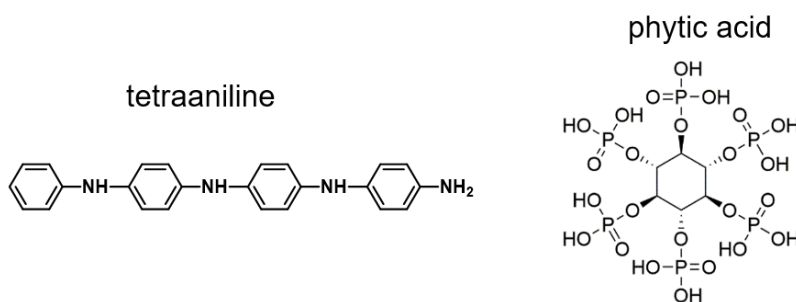


Figure 1. The chemical structure of a phytic acid molecule and tetraaniline molecule.

2. EXPERIMENTAL SECTION

2.1 Materials

A commercial epoxy resin E44 and matched amine curing agent were provided by Yunda Chemical Co. Ltd. Ammonium persulfate (APS), 4-aminodiphenylamine, ammonia solution, and phytic acid solution (70% in H₂O) were purchased by Aladdin Industrial Corporation. Q235 steel material was used as the substrate in this study. Hydrochloric acid, acetone, and absolute ethanol were provided by Sinopharm Chemical Reagent Co. Ltd.

2.2 Preparation of TANI and PATA nanoparticle

The TANI was prepared by following previous literature [9]. 60 mmol of 4-aminodiphenylamine was fully dissolved in the 75 mL of 1 M HCl, 300 mL of acetone, and 300 mL of deionized water in an ice bath. Then, 40 mmol of APS in 150 mL of 1M HCl solution was added dropwise into the above-mentioned mixture for 1 h. Continuing the reaction for 3 h, the semi-product was filtered to collect, and then dedoped via dissolved in 300 mL deionized water and 50 mL of ammonia solution with vigorous stirring for 5 h. The dry TANI powder was obtained by filtration and washing repeatedly by deionized water and drying to a constant weight at 40 °C for 48 h. 10 mg of TANI powder and 50 mL of 0.02 M phytic acid solution were mixed under ultrasonic irradiation for 3 mins. The green PATA slurry was obtained by centrifugation. Finally, the dry PATA powder was dried to constant weight as a powder in vacuum at 40 °C for 72 h.

2.3 Preparation of PATA/EP composite coatings

The composite coatings containing 0.1, 0.5, and 1.0 wt% of PATA nanoparticles were prepared. The related coatings with pure epoxy, 0.1 wt%, 0.5 wt%, and 1.0 wt% were marked as pure EP, PATA_{0.01}/EP, PATA_{0.25}/EP, and PATA_{0.5}/EP. The E44, PATA, and ethanol solution were mixed and dispersed using a high-speed agitator at room temperature. After ethanol was removed via rotatory evaporation, the coating mixture was coated on the Q235 steel electrodes surface via a bar coater. The prepared coating samples were cured for 1 d at 25 °C until the coating mixture was completely cured.

2.4 Characterization

2.4.1 Characterization of the prepared PATA nanoparticle

The scanning electron microscope (SEM) patterns of PATA nanoparticles and fracture surface of coatings were obtained by HITACHI S4800 (Japan). And the morphologies of PATA nanoparticles were also performed by the scanning probe microscope (SPM, Dimension 3100). The X-ray photoelectron spectroscopy (XPS) and Raman results of PATA were performed by AXIS UTLTRA DLD (England) and Via Reflex (England). After 60 days of immersion, the corroded coating electrode

was investigated with SEM (HITACHI S4800, Japan) and energy dispersive spectroscopy (EDS, Japan).

2.4.2 Electrochemical tests of PATA/epoxy composite coatings

The open circuit potential (OCP) and electrochemical impedance spectroscopy (EIS) results of PATA/EP coatings were obtained via CHI-660E electrochemical workstation (China). The traditional three-electrode system was employed: coating electrode: working electrode; reference electrode: saturated calomel electrode; counter electrode: platinum plate electrode). The EIS data point was detected in the range of 10^{-2} – 10^5 Hz with an amplitude of 20 mV. The scanning vibrating electrode technique (SVET) test instrument was from VersaSCAN micro scanning electrochemical workstation (AMETEK, USA). To characterize the active corrosion protection ability of coatings, a visible artificial defect with 2mm of length was scratched on the coating surface via a scalpel. The amplitude of 20 μm of microelectrode probe was 30 μm with a frequency of 80Hz (scanning region: 2 mm^2).

3. RESULTS AND DISCUSSION

3.1 Characterization of PATA nanoparticle

The SEM is employed to analyze the morphologies and distribution of PATA nanoparticles. As shown in Figure 2a and 2b, a great deal of well-dispersed nanoparticles with a size of 60–120 nm is discovered. Besides, the morphology and distribution state could also be verified by SPM results. From the SPM image (Figure 2c and 2d), the PATA nanoparticles show a well-dispersed spherical morphology, and the diameter of particles are approximately 65–100 nm, which agreed with the analysis of SEM results.

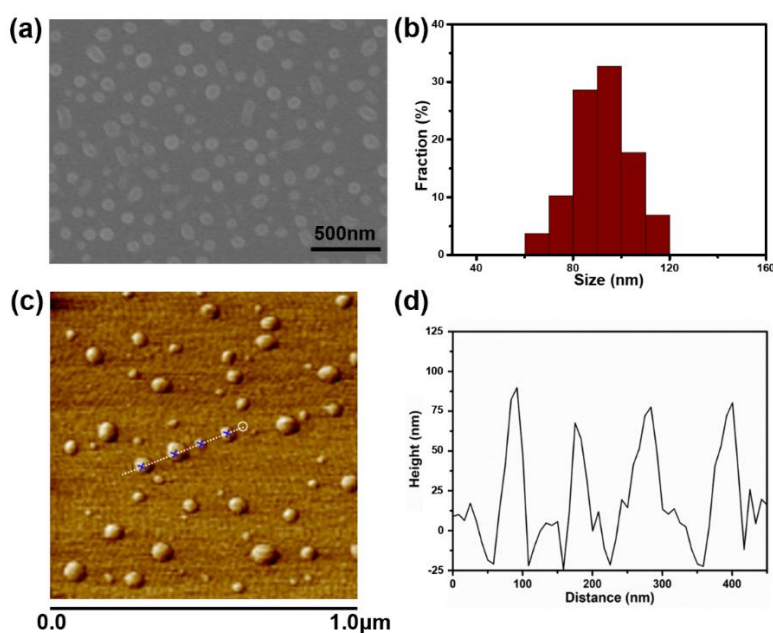


Figure 2. Morphology and size of PATA nanoparticles: (a) SEM image; (b) grain size; (c) SPM image; (d) the height of selected zone.

The XPS spectra of the PATA nanoparticle is shown in Figure 3. Figure 3a exhibits that the C 1s core level spectrum can be decomposed into four peaks. The C–O peak at 286.4 eV is from phytic acid. The second peak (C–N⁺/C=N⁺) at 285.2 eV is assigned to the carbon atoms bonded to positively charged nitrogen [8]. The last two peaks at 284.4 eV (C–N and C=N) and 283.9 eV (C–C or C–H) are assigned to the backbone of TANI-PA molecule. Figure 3b shows that the peak of N 1s core level spectrum is divided into three peaks. The first peak at 398.7 eV (N⁺) is attributed to positively charged nitrogen [19]. The atomic composition and the quantitatively doping level are listed in Table 1. The doping level of PATA nanoparticle is obtained via the ratio of positively charged nitrogen content to the entire nitrogen content. The doping level of PATA nanoparticle reaches 19%, confirming PATA is in its self-doped conducting form. Also, the nitrogen contribution at 397.7 eV and 396.4 eV are ascribed to benzenoid diamine nitrogen (–NH–) and quinoid di-imine (–N=), respectively. Figure 3c exhibits that the peak of O 1s also can be decomposed into three peaks, which are all attributed to phytic acid structure, including O–C at 530.9 eV, –OH at 529.6 eV, and O–P at 528.4 eV. For Figure 3d, the P 2p peak at 133.9 eV is assigned to H₂PO₄¹⁻ in phytic acid structure [20].

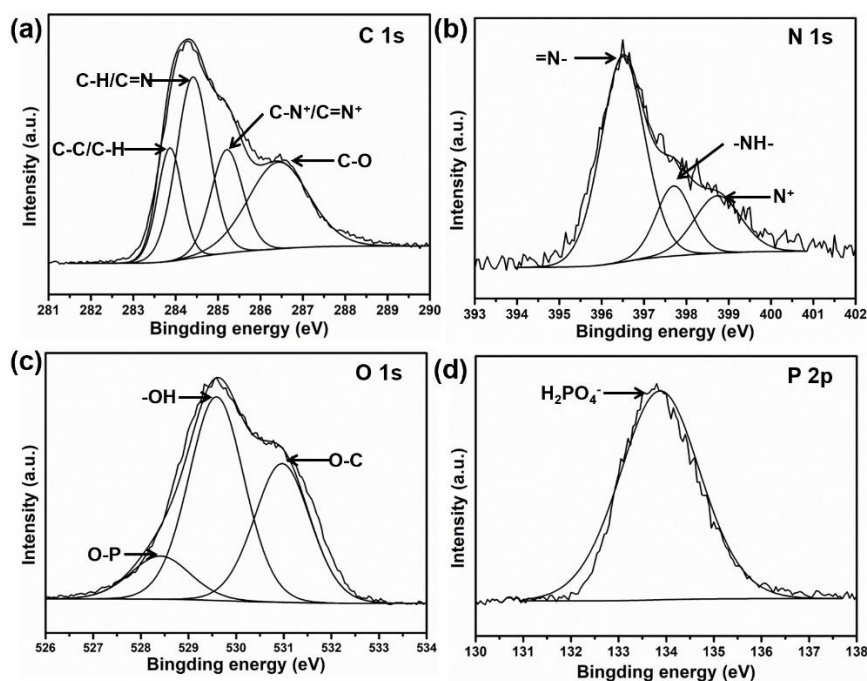


Figure 3. (a) C 1s, (b) N 1s, (c) O 1s, and (d) P 2p XPS spectra of the synthesized PATA nanoparticles.

Table 1. The elemental analysis of PATA nanoparticle and doping ratio calculated by XPS.

Sample	Atomic composition (%)				Doping level	
	C	N	C	P	P/N	N ⁺ /N
PATA	67.81	23.72	7.35	1.12	0.13	0.19

Figure 4 depicts the Raman spectrum of the PANI-PA. The strong peak at 1619 cm⁻¹ is attributed

to the C=N stretching vibration in quinonoid rings [7]. The peaks at 1591 cm^{-1} and 1563 cm^{-1} are due to the C=C stretching vibration of a benzenoid and quinonoid ring in PATA backbone. The obvious peak at 1337 cm^{-1} is from protonated imine in PATA molecular chain and the strong peak at 1178 cm^{-1} is attributed to the C-H bending vibration of the quinonoid ring structure [21]. These two characteristic peaks confirmed the synthesized PATA nanoparticle that the phytic acid has been doped with TANI successfully, which is following the analysis of XPS results.

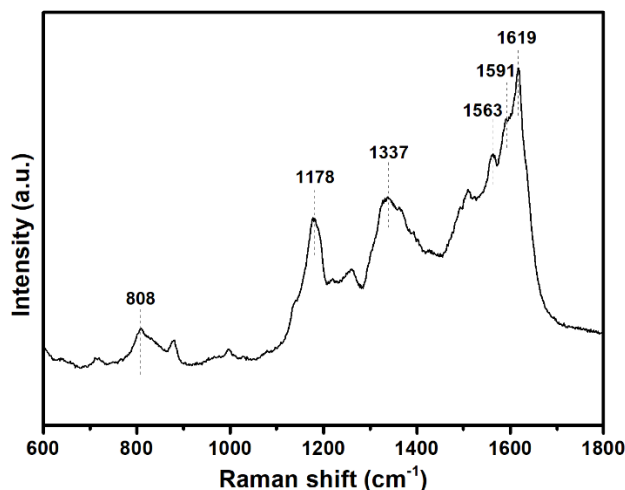


Figure 4. Raman spectrum of the synthesized PATA nanoparticles.

3.2 Characterization of PATA/EP coating

To characterize the dispersion state of PATA nanofiller in the epoxy matrix, Figure 5 shows the SEM images of fracture surfaces of different coatings. As seen in pure EP (Figure 5a), there are many clear defects on the fracture surface such as tiny air bubbles and tube-like traces. Dealing with these inevitable tiny bubbles and faults is the key to improving the overall corrosion resistance of the coating. By contrast, as shown in Figure 5b and 5c, when the content of PATA nanoparticles is increased to 0.25 wt%, micro defects can be hard to observe on the fracture surface of the PATA_{0.25%}/EP sample, revealing that this nanoparticle can be able to fill the microcavities in the EP coating efficiently. However, when the content of PATA nanoparticles researches 0.5 wt%, we can observe much more tiny holes and wrinkles on the fracture surface (Figure 5d). It is because the overuse of nanoparticles induced more microcrack spread. Hence, the SEM results of fracture surfaces confirm that 0.5 wt% of PATA nanoparticles possess the best dispersion state in the epoxy resin matrix.

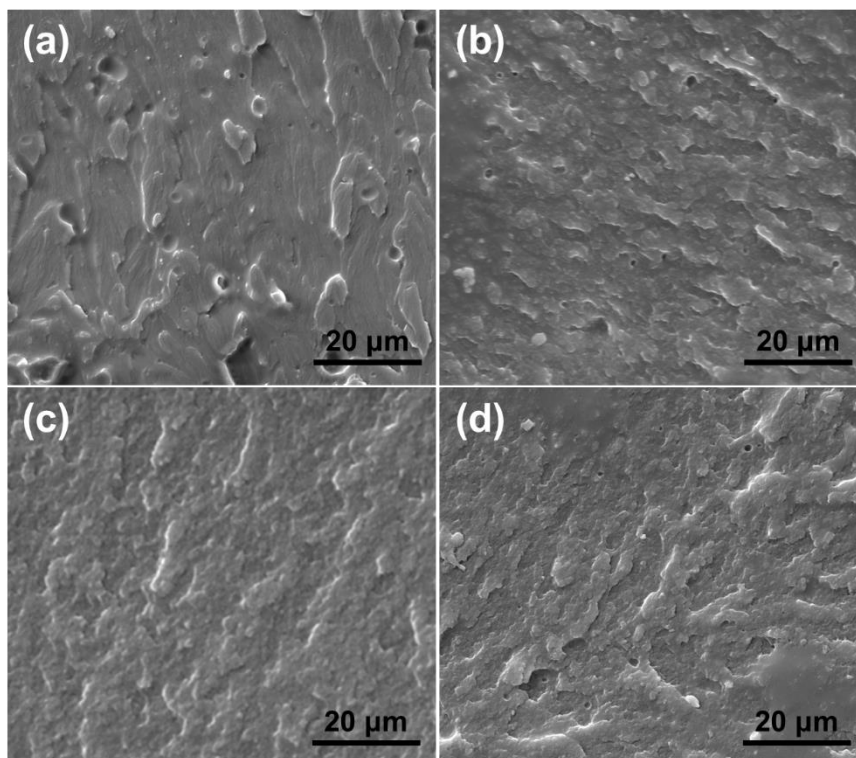


Figure 5. SEM images of fracture surface for (a) pure EP, (b) PATA_{0.1%}/EP, (c) PATA_{0.25%}/EP and PATA_{0.5%}/EP coatings.

3.3 OCP tests

The OCP results for different coating samples in 3.5 wt% NaCl solution are depicted in Figure 6. For pure EP sample, OCP values decline gradually from -532 mV to -627 mV after immersion of first 20 days, indicating that the corrosive species have infiltrated gradually into the epoxy matrix. Nevertheless, the OCP values of pure EP increase steadily from -627 mV to -498 mV during the next 40 days because of the rust accumulation beneath the organic coating [16, 22]. Also, for the overall immersion process, the lowest-level OCP values (~ 550 mV) reveal the weak corrosion resistance of pure EP compared to other composite coatings. The OCP results of coatings PATA_{0.1%}/EP and PATA_{0.5%}/EP decrease gradually over time, revealing that the corrosive species has also permeated steadily into these coatings. By contrast, despite the OCP value of PATA_{0.5%}/EP fluctuates slightly at initial immersion time, its value increases steadily and eventually reaches 115 mV after 60 days of immersion. By comparing the overall level of OCP value of all coating samples, it is found that the OCP value of epoxy coating loaded with PATA filler is higher than that of pure EP sample, especially the PATA_{0.25%}/EP coating. The OCP value of PATA_{0.25%}/EP coating increases gradually and its OCP result is higher than the rest of the coatings after 23 days of immersion. The positive shift of the OCP value while maintaining a relatively high level reveals that a stable passivation film is formed on the surface of the Q235 steel beneath the epoxy coating.

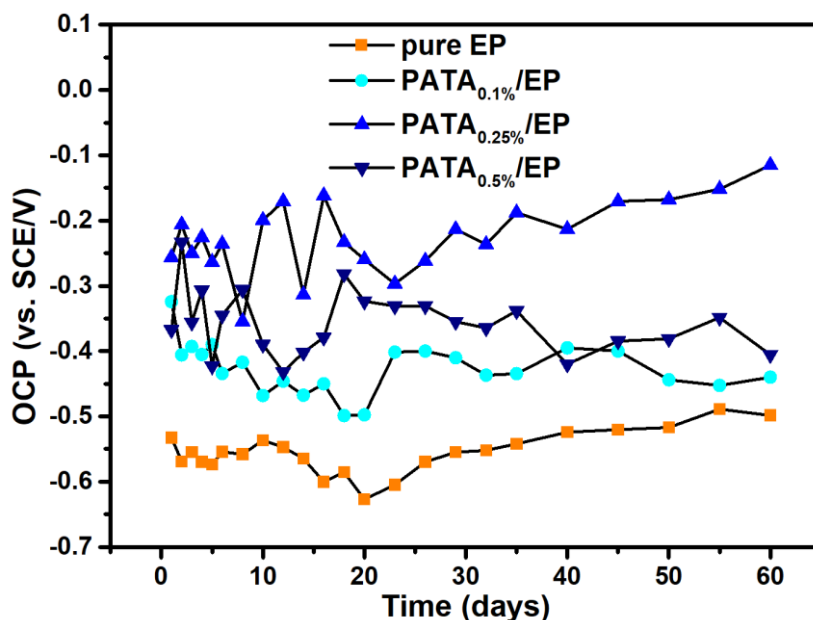


Figure 6. OCP results of different coatings tested in 3.5wt% NaCl solution during 60 days of immersion.

3.4 EIS analysis

EIS technique is used to study the corrosion protection ability of the selected composite coatings. The Bode and phase angle plots of the samples tested in 3.5 wt% NaCl solution for 60 days are presented in Figure 7. For phase angle results, the peak located in the high frequency is attributed to the response of the capacity and resistance of the coating, while the peak appearing at the low or medium frequency is related to the response of the corrosion reaction [23, 24]. In terms of pure EP, two peaks in Figure 7b are seen after 20 days of immersion, which is evidence of coating failure. Such a quick failure of the coating is derived from the internal micro defects of the coating caused by the coating matrix curing process. However, the second time constant is not obvious for PATA/EP composite coating even after 60 days of immersion as seen in Figure 7d, which demonstrates that PATA filler strongly decreases the coating micro defects and improves its impermeability.

Also, the impedance values at the lowest frequency ($f = 10$ mHz) can be regarded as a semiquantitative parameter of the barrier property of the organic coating. It could be seen that the impedance values for pure EP, PATA_{0.1%}/EP, and PATA_{0.5%}/EP coatings drop greatly during the overall immersion periods. Generally, the decrease in impedance values is due to the penetration of corrosion solution into the epoxy coating matrix. When the water absorption coating reaches saturation, the organic coating almost loses its barrier ability for metal material. For pure EP, the impedance value decreases rapidly from $1.97 \times 10^8 \Omega \text{ cm}^2$ to $6.39 \times 10^6 \Omega \text{ cm}^2$ after 20 days of immersion because of the weak barrier ability of pure epoxy coating. When 0.1% PATA filler is added to the epoxy coating, the impedance value decreases from $1.97 \times 10^8 \Omega \text{ cm}^2$ to $6.39 \times 10^6 \Omega \text{ cm}^2$ at the initial immersion period, showing that the addition of fillers can significantly enhance the barrier ability of the coating. In the case

of the PATA_{0.25%}/EP coating, its impedance remains at a relatively high-level value ($\sim 10^8 \Omega \text{ cm}^2$) for the entire immersion time, which is higher than pure EP and PATA_{0.1%}/EP samples. However, when the more content of PATA filler (reach up to 0.5 wt%) is added to the epoxy coating, its impedance change trend during the entire immersion time is similar as PATA_{0.1%}/EP sample and its final impedance only reaches $9.95 \times 10^6 \Omega \text{ cm}^2$, which is much lower than the PATA_{0.25%}/EP sample by ~ 2 orders of magnitude. This may be because a large number of fillers formed agglomerations in the coating matrix and generated micro-defects. By contrast, the as-prepared PATA_{0.25%}/EP coating has a superior corrosion resistance for the Q235 steel substrate.

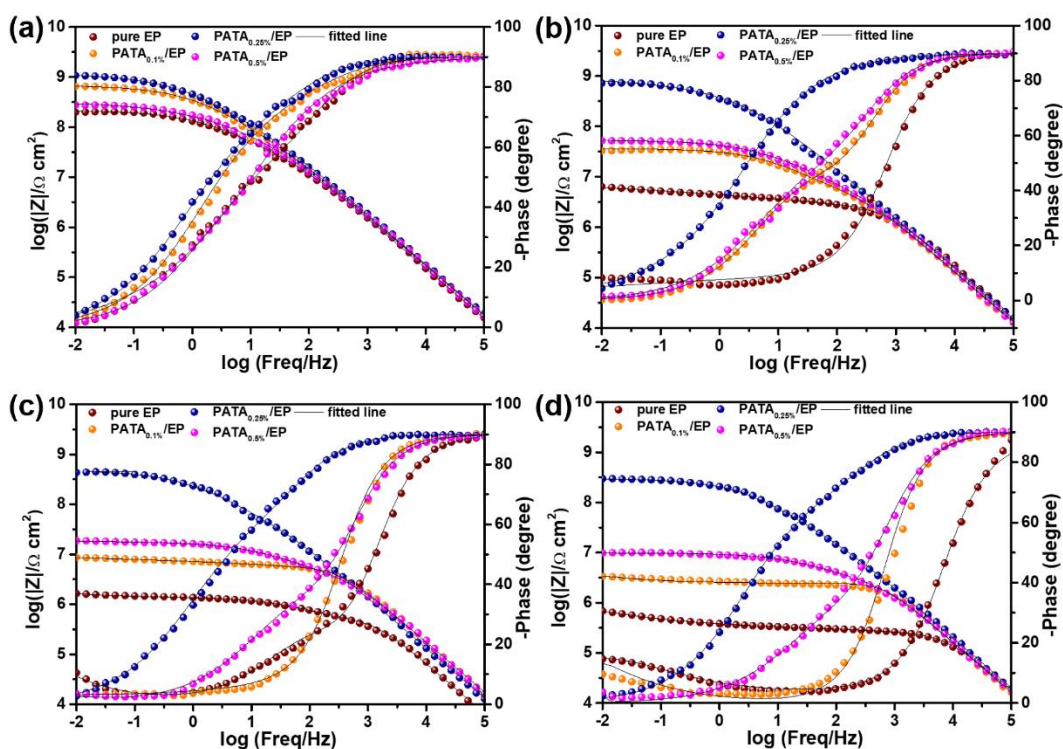


Figure 7. Bode and phase angle plots of different coatings with immersion in 3.5 wt % NaCl solution: (a) 1 day, (b) 20 days, (c) 40 days and (d) 60 days.

Furthermore, the EIS results are fitted through ZSimpWin 3.30 software using the equivalent circuits depicted in Figure 8. In the fitted equivalent circuits, R_s , R_p , and R_{ct} represent the solution resistance, the pore resistance, and charge transfer resistance, respectively. The constant phase element presents the deviation from the capacitance element marked as ‘Q’ [25]. Q_c and Q_{dl} relate to the coating capacitance and coating/steel double-layer capacitance. Also, the Warburg component (Z_w) element could be related to the corrosion diffusion behavior [26].

R_p decreases with increasing immersion time because of the penetration of the corrosive species and the degradation of the epoxy coating [27]. Figure 9a presents the fitted results of pore resistance (R_p) for different coatings in 3.5 wt% NaCl solution after 60 days immersion. In terms of pure EP, the R_p value declines from $1.60 \times 10^7 \Omega \text{ cm}^2$ to $7.49 \times 10^4 \Omega \text{ cm}^2$. For composite epoxy coating, PATA_{0.1%}/EP,

PATA_{0.25%}/EP and PATA_{0.5%}/EP have the pore resistance values of $2.45 \times 10^6 \Omega \text{ cm}^2$, $1.53 \times 10^7 \Omega \text{ cm}^2$ and $6.41 \times 10^5 \Omega \text{ cm}^2$ of immersed final period. PATA_{0.25%}/EP coating sample is around 1~2 order of magnitude higher than other samples, revealing that PATA_{0.1%}/EP and PATA_{0.5%}/EP have relatively weak barrier property after the immersion of 60 days.

Figure 10 presents the values of coating capacitance (Q_c) for different coatings in 3.5 wt% NaCl solution after 60 days immersion. Q_c shows the absorption ability of corrosive species, and the organic film is apt to breach with the attack of corrosive species, which results in the loss of the barrier function [16]. The corrosive species permeated into the coating matrix result in the increase of Q_c , owing to NaCl solution have a higher dielectric constant than coating matrix. As the coating is penetrated by NaCl solution, the Q_c values for pure EP, PATA_{0.1%}/EP, and PATA_{0.5%}/EP have increased to $1.18 \times 10^{-10} \text{ F cm}^{-2}$ and $9.67 \times 10^{-11} \text{ F cm}^{-2}$ and $9.92 \times 10^{-11} \text{ F cm}^{-2}$ after immersion of 60 days, respectively. Nevertheless, the final Q_c value ($7.97 \times 10^{-11} \text{ F cm}^{-2}$) of PATA_{0.25%}/EP is relatively lower than those of the above three coatings', revealing only a small amount of NaCl solution attacked into the PATA_{0.5%}/EP coating, indicating the superior anti-corrosion property.

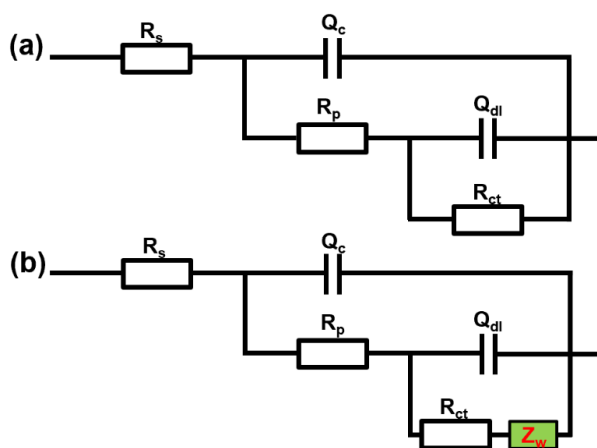


Figure 8. Equivalent circuit fitted models with immersion in 3.5 wt% NaCl solution for 60 days.

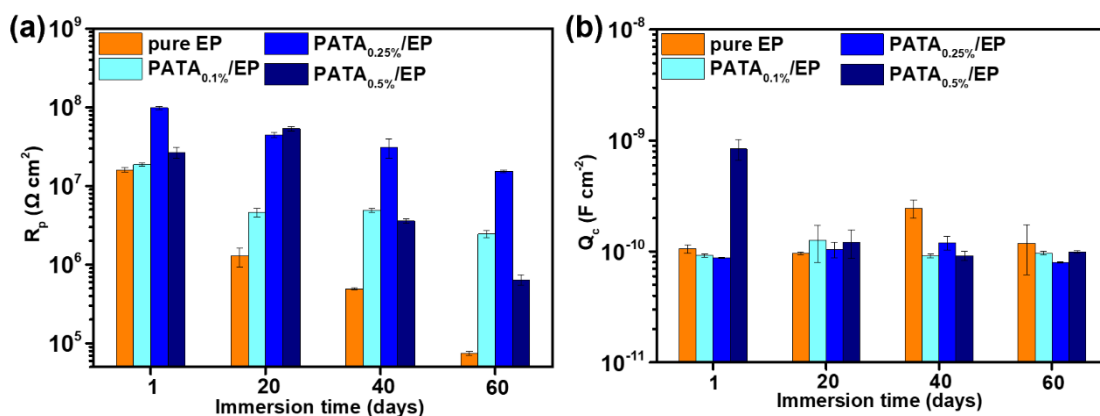


Figure 9. Fitted results of pore resistance (R_p) and coating capacitance (Q_c) for different coatings in 3.5 wt% NaCl solution for 60 days.

3.5 Corrosion product analysis

As seen in Figure 10 and Table 2, the corroded steel surface of pure EP (Figure 10a) mainly consists of Fe (87.67%), O (9.18%), and Cl (3.45%), which reveals that lots of water and corrosive species has reached the metal substrate. In terms of PATA_{0.25%}/EP, the content of Cl (0.16%) for the corroded steel surface (Figure 10b) is much lower than that of pure EP and the steel surface of pure EP shows a cleaner substrate surface than PATA_{0.25%}/EP. These results demonstrate that only a small amount of corrosion occurred on the surface of the substrate. Also, it is worth noting that 0.85% of P element is found on the surface of this sample, indicating that phosphorus-containing compounds are formed during the corrosion reaction. According to SEM and EDS results, the epoxy coating containing 0.25 wt% of PATA nanoparticles has good barrier properties and passivation effects.

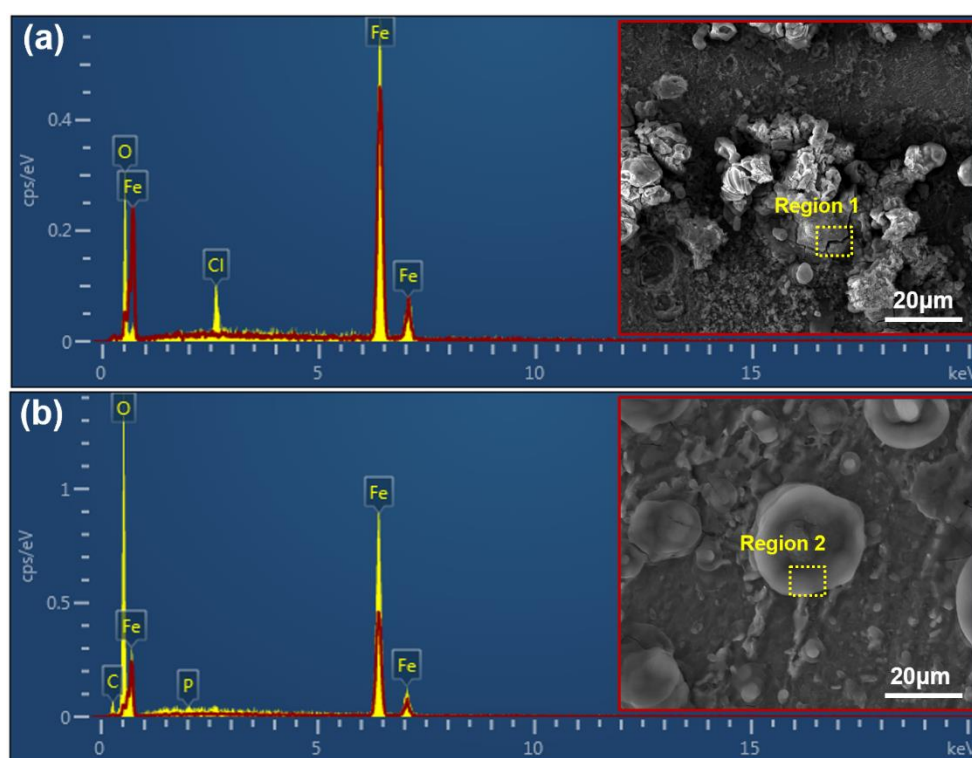


Figure 10. Images and EDS results of the corroded surfaces of pure EP (Region 1) and PATA_{0.25%}/EP (Region 2) after 60 days immersion in a 3.5 wt% NaCl solution. All samples are the bare steel surfaces with rust after removing the coating.

Table 2. The elemental analysis of TANI nanofiber, its molecular formula, and Cl/N ratio by XPS.

Sample	Fe	O	C	Cl	P
pure EP	87.67	9.18	-	3.45	-
PATA _{0.25%} /EP	81.33	15.32	2.34	0.16	0.85

3.6 SVET analysis

For further study of the active corrosion protective ability of the coatings with PATA nanoparticles, the SVET technique is employed for investigating the local area corrosion activities [28, 29]. Generally, the electrochemical reactions at the man-made scratch position resulted in a significant enhancement in anodic current density. Figure 11 shows the current density distribution diagram after 1 h and 24 h with immersion in 3.5 wt% NaCl solution for pure EP and PATA_{0.25%}/EP. As shown in Figure 11a and 11c, the similar current density distribution of colorful images are observed, revealing pure EP and PATA_{0.25%}/EP coating have the semblable original anodic current density after 1 h of immersion in 3.5 wt% NaCl solution. After 24 hours of exposure to 3.5 wt% NaCl solution, the corrosion current density of pure EP increases (Figure 11b), revealing the deterioration of the corrosion reaction at the scratch position. By contrast, there is no obvious response of anodic corrosion current signals (Figure 11d) for the PATA_{0.25%}/EP coating, demonstrating corrosion activity has suppressed successfully with the existence of PATA nanoparticles.

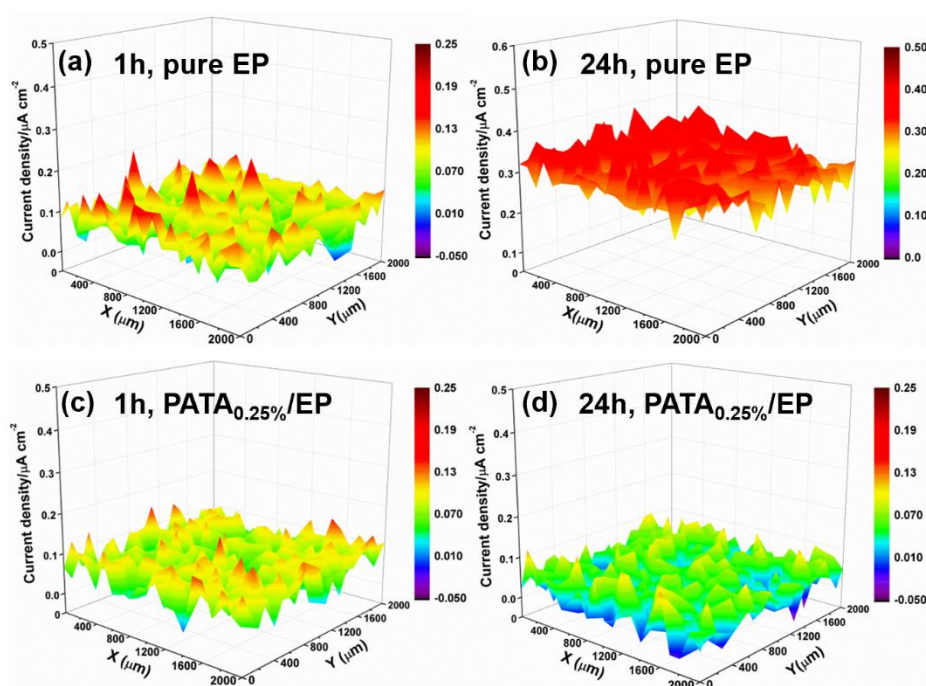


Figure 11. 3D current density distribution of coated Q235 steels immersed in 3.5wt % NaCl solution for 1 h and 24 h. (a, b) pure EP and (c, d) PATA_{0.25%}/EP, unit of current density: $\mu\text{A cm}^{-2}$.

4. CONCLUSIONS

Herein, a phytic acid-doped tetraaniline (PATA) nanoparticle was prepared by assembly chemistry. The nanoscale makes it suitable as a processable additive for epoxy coatings to be applied to the anticorrosion field. Epoxy coating blended with 0.1 wt%, 0.25 wt%, and 0.5 wt% of PATA nanoparticles was successfully prepared. The results of the OCP test, EIS test, and SVET technique

revealed that epoxy coating blended with 0.25 wt% of PATA nanoparticles exhibited excellent corrosion protective ability. Moreover, this work offers fire-new thinking to obtain the processable nanoscale polymer and further potential applications as a corrosion inhibitor for improving the corrosion resistance of epoxy coatings.

CONFLICTS OF INTEREST

All authors declare no competing financial interest.

References

1. X. Li, D. Zhang, Z. Liu, Z. Li, C. Du, C. Dong, *Nature*, 527 (2015) 441.
2. F. Zhang, P. Ju, M. Pam, D. Zhang, Y. Huang, G. Li, X. Li, *Corros. Sci.*, 144 (2018) 74.
3. A. Kalendová, I. Sapurina, J. Stejskal, D. Veselý, *Corros. Sci.*, 50 (2008) 3549.
4. C. Ocampo, E. Armelin, F. Liesa, C. Alemán, X. Ramis, J. I. Iribarren, *Prog. Org. Coat.*, 53 (2005) 217.
5. J. Martins, T. Reis, M. Bzzaoui, E. Bzzaoui, L. Martins, *Corros. Sci.*, 46 (2004) 2361.
6. S. Qiu, W. Li, W. Zheng, H. Zhao, L. Wang, *ACS Appl. Mater. interfaces*, 9 (2017) 34294.
7. S. Qiu, C. Chen, M. Cui, W. Li, H. Zhao, L. Wang, *Appl. Surf. Sci.*, 407 (2017) 213.
8. Y. Hao, L.A. Sani, T. Ge, Q. Fang, *Appl. Surf. Sci.*, 419 (2017) 826.
9. T. Liu, J. Li, X. Li, S. Qiu, Y. Ye, F. Yang, H. Zhao, *Prog. Org. Coat.*, 128 (2019) 137.
10. T. Liu, Y. Liu, Y. Ye, J. Li, F. Yang, H. Zhao, L. Wang, *Prog. Org. Coat.*, 132 (2019) 455.
11. L. Zang, Y. Che, J.S. Moore, *Acc. Chem. Res.*, 40 (2009) 1596.
12. H. Kim, T.-G. Kim, J.-W. Park, *Macromol. Res.*, 21 (2013) 815.
13. B.O. Alexander, G. Wu, J.S. Haataja, B. Felicitas, F. Natalie, A.M. Seddon, R.L. Harniman, R.M. Richardson, I. Olli, Z. Xi, *J. Am. Chem. Soc.*, 137 (2015) 14288.
14. W. Lv, J.T. Feng, W. Yan, C.F.J. Faul, *J. Mater. Chem. B*, 2 (2014) 4720.
15. W. Lyu, J. Feng, W. Yan, C.F. Faul, *J. Mater. Chem. C*, 3 (2015) 11945.
16. F. Yang, T. Liu, J. Li, H. Zhao, *Int. J. Electrochem. Sci.*, 13 (2018) 6843.
17. T. Liu, H. Zhao, J. Li, D. Zhang, W. Zheng, L. Wang, *Corros. Sci.*, 168 (2020) 108555.
18. L. Yang, H. Liu, N. Hu, *Electrochem. Commun.*, 9 (2007) 1057.
19. M.G. Han, S.K. Cho, S.G. Oh, S.S. Im, *Synth. Met.*, 126 (2002) 53.
20. X. Cui, Q. Li, Y. Li, F. Wang, G. Jin, M. Ding, *Appl. Surf. Sci.*, 255 (2008) 2098.
21. R. Mažeikienė, V. Tomkutė, Z. Kuodis, G. Niaura, A. Malinauskas, *Vib. Spectrosc.*, 44 (2007) 201.
22. F. Yang, X. Li, Z. Dai, T. Liu, W. Zheng, H. Zhao, L. Wang, *Int. J. Electrochem. Sci.*, 12 (2017) 7469.
23. C. Liu, H. Zhao, P. Hou, B. Qian, X. Wang, C. Guo, L. Wang, *ACS Appl. Mater. Interfaces*, 10 (2018) 36229.
24. C. Liu, P. Du, H. Zhao, L. Wang, *ACS Appl. Nano Mater.*, 1 (2018) 1385.
25. J. B. Jorcin, M.E. Orazem, N. Pébère, B. Tribollet, *Electrochim. Acta*, 51 (2006) 1473.
26. M. Cui, S. Ren, H. Zhao, Q. Xue, L. Wang, *Chem. Eng. J.*, 335 (2017) 255.
27. T. Liu, J. Wei, L. Ma, S. Liu, D. Zhang, H. Zhao, *Prog. Org. Coat.*, 151 (2021) 106109.
28. M. Mouanga, F. Andreatta, M.E. Druart, E. Marin, L. Fedrizzi, M.G. Olivier, *Corros. Sci.*, 90 (2015) 491.
29. Y.H. Liu, J.B. Xu, J. T. Zhang, J.M. Hu, *Corros. Sci.*, 120 (2017) 61